Maradin's Micro-Mirror – System Level Synchronization Notes

Sharon Hornstein, Tal Langer, Menashe Yehiel, Matan Naftali
Maradin Ltd., 2 HaCarmel St., Yokne'am, 20692, Israel

Abstract
Maradin's novel MEMS-based micro-mirror is designed to operate as part of laser beam steering projection systems. This paper presents some issues concerning the use of scanning micro-mirrors for such applications, and explains how to overcome image distortions that emerge when micro-mirrors are used for projection of light.

Keywords
2D MEMS scanning mirrors; MOEMS; Head-Up-Displays; Pico-Projectors; Gesture Recognition

1. Introduction
MEMS–based laser steering projectors that enable to display large images from within mobile electronic devices are drawing much attention both in the industrial community as well as at potential end-users. The miniature size of the light-engine that projects a single light source forming a large image that could be projected onto an arbitrary screen makes it suitable for a wide range of future products that comprise the micro-mirror as an additional component and enhance their performance. Moreover, scanned laser projectors have an infinite focus, which means that the projected image is focused at any depth, while increasing the horizontal distance between the projector and the screen yields in an increase of the image size.

A few examples of such systems, that comprise of a MEMS-based micro-mirror having two axes for rotation, can be found at [1],[4],[5],[6],[8]. The evolution of the high-resolution scanners can be noticed when the early inventions of scanning mirrors [2] can be compared to the efforts that are currently at the edge of the technology [3], that include the development of a 3D display based on a high-resolution projector. These papers focus primarily on the mechanical and electrical challenges required for a high-resolution image, but do not refer to any distortions that may result in the projected image. This issue has minor references in the literature. Specht et al.[7] is one of the few works that treat the distortions caused by projection of images using micro-mirrors. They discuss the relationship between parameters characterizing the scan engine and their influence on image quality, and treat the distortions obtained in the projected images. However, to the best of the authors' knowledge, there is no comprehensive study of the root-cause of these distortions and no detailed algorithms for compensation of such phenomena.

This paper focus on the technological challenges required for compensating of the optical distortions that are caused at laser-projected images using micro-mirror projectors. More specifically, we focus on laser synchronization algorithm that should be treated at system-level integration. The paper is organized as follows. Chapter 2 deals with synchronization of a horizontal projected line, and Chapter 3 focuses on the compensation of the pincushion distortion effect.

2. A Single Line Synchronization

2.1. Problem Definition

The horizontal line that is projected on the screen is created from a traveling light point that is reflected from the mirror. The mirror rotates around the horizontal axis with constant frequency, which can be mathematically described by the following sinusoidal motion:

$$\theta^{M,x}(t) = \theta^{M,x}_{peak}\cos(\omega_n t) = \frac{1}{2}\theta^{O_p,x}_{peak}\cos(\omega_n t) \quad (1)$$

Where $\omega_n = 2\pi f_n$ [rad/sec] is the resonance frequency of the mirror (in the x direction) and $\theta^{M,x}_{peak}$ is the mechanical maximum amplitude of the x axis. Differentiation of the angular position vector with respect to time yields:

$$\dot{\theta}^{M,x}(t) = \omega_n\theta^{M,x}_{peak}\sin(\omega_n t) = \frac{1}{2}\omega_n\theta^{O_p,x}_{peak}\sin(\omega_n t) \quad (2)$$

Eq. (2) shows that the velocity of the mirror in the x axis is time dependent, and implies that the projection speed of the pixels depends on their location along the line.

The main concern of this work is to define the time vector t in Eqs. (1)-(2), such that the location of the mirror can be defined in terms of the pixel index along the horizontal line.

2.2. Parameters Definition
There are a few parameters that define the angular motion of the mirror and influence the laser synchronization. Table 1 summarizes these parameters.

Table 1: Horizontal Scan Parameters

Parameters	Definitions
N_h	No. of pixels (horizontal)
f_n [Hz]	Natural frequency (horizontal)
$\theta^{M,x}_{peak}$ [rad]	Maximum ***horizontal*** Mechanical Angle - Peak

We define two different angles that correspond to the mechanical angle of the axis $\left(\theta^{M,x}_{peak}\right)$ and the optical angle of the projected line $\left(\theta^{O_p,x}_{peak}\right)$. The relationship between these angles is described using the following: $\theta^{M,x}_{peak} = \theta^{O_p,x}_{peak}/2$. We note that the optical angle $\theta^{O_p}_{peak}$ is measured between the optical center and one edge of the projected line.

2.3. Algorithm for a Single Line Synchronization

The resonance frequency in the horizontal direction determines the time required to project a single line, via the definition of its period. During one oscillating cycle, the mirror projects two horizontal lines. Therefore, the time required to project a single horizontal line is calculated via:

$$\text{Time per Line}[\text{sec}] = 1/2f_n \quad (3)$$

Each horizontal line is represented by a series of pixels, which are spanned along the line. Figure 1 depicts a schematic sketch of the line composed of N_h pixels.

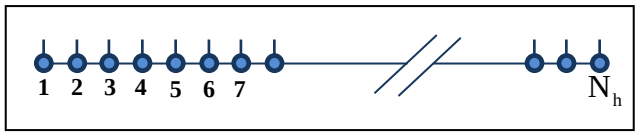

Figure 1: Schematic sketch of a horizontal line with N_h pixels

We define a vector for the pixel index, which has N_h components:

$$P_{ind} = [1, 2, ..., N_h] \quad (4)$$

Following the description above, the projected horizontal line is created from the rotational motion of the x-axis. The optical angle is defined as the distance from one edge of the line to the optical center. Figure 2 depicts the Schematic sketch of a horizontal line and the definition of $\theta_{peak}^{O_p,x}$.

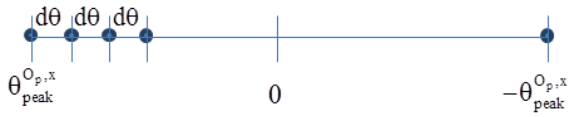

Figure 2: Schematic sketch of a horizontal line, spanned along $2\theta_{peak}^{O_p,x}$ degrees

Similarly to the pixel index vector, we define a vector for the angle index, which have N_h components as well. Any two successive components of the angle vector are linearly spaced with the definition of $d\theta = \theta(i+1) - \theta(i)$, and we assume that $\theta(1) = \theta_{peak}^{O_p}$. The difference $d\theta$ is defined as :

$$d\theta[\text{rad/pixel}] = 2\theta_{peak}^{O_p,x} / (N_h - 1) \quad (5)$$

Eq. (5) defines the ratio between the maximal optical angle and the number of pixels in the horizontal direction.

Before calculating the time required to project a single pixel based on the sinusoidal profile, we show a simplified calculation for a case where the mirror has a constant speed. In that case, the time required to project a single pixel can be performed based on the following formula:

$$dt_{lin}[\text{sec}] = \text{Time per Line} / (N_h - 1) \quad (6)$$

The time difference between any two successive pixels is calculated from Eq. (2), where we use $\dot{\theta} = d\theta/dt$. We isolate the known dt and obtain:

$$dt_{sin}[\text{sec}] = d\theta / \theta_{peak}^{O_p,x} \omega_n \sin(\omega_n t) \quad (7)$$

We can use Eq. (5) for $d\theta$ and obtain the following:

$$dt_{sin} = 2/\omega_n (N_h - 1) \sin(\omega_n t) \quad (8)$$

We note that Eq. (8) is a nonlinear equation, which seem to be dependent in two variables: dt_{sin} and t. Since the distribution of the dt's is not constant along the line, we define the time vector t as follows, using the formulation $t(i) = t(i-1) + dt_{sin}(i)$. The solution of this equation was performed using the nonlinear bi-section method.

2.4. *An example case of a line synchronization*

We refer to Table 1 and use the following values for the parameters: $N_h = 854, f_n = 10250[\text{Hz}]$, $\theta_{peak}^{M,x} = 9^0 \pi/180$. The calculation for the linear distribution of dt from Eq. (6) yields $dt_{lin} = 5.718 \cdot 10^{-8}[\text{sec}]$.

We used the nonlinear formula in Eq. (8) and calculated the time difference dt_{sin} for each two successive pixels. Figure 3 depicts the graphical comparison of the linearly-spaced pixels (with constant time difference; blue curve) and the unevenly-spaced pixels due to the sinusoidal velocity profile, which yields a variable dt (red curve). We note that the linear dt curve seems to be an 'average' of the non-constant time difference. The minimal point of the dt_{sin} is $3.65 \cdot 10^{-8}[\text{sec}]$.

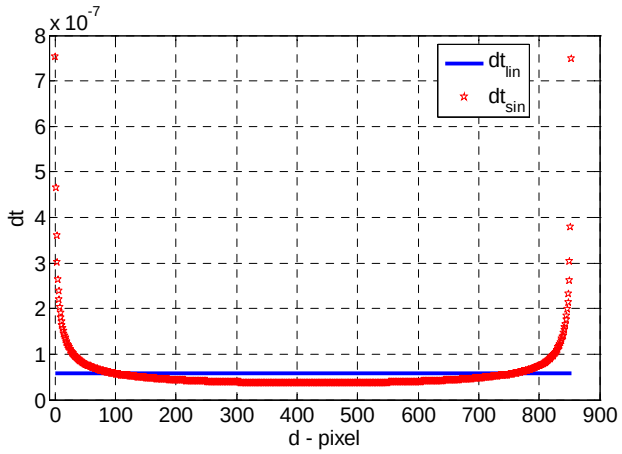

Figure 3: Comparison between the variable scan speed (red) and constant scan speed (blue)

3. One Field Synchronization

3.1. *General Description*

When projecting a series of horizontal lines which have variable distance from the optical axis, there exists an optic distortion, which is expressed by deviation from rectilinear projection along the edges. This phenomenon is visible when straight lines that do not go through the center of the image are bowed towards the center point of the image. When both horizontal and vertical lines are bowed inwards, a pincushion-like shape is visible. Figure 4 shows a typical symmetric pincushion distorted image.

Figure 5 was obtained from a simulation analysis of the projected picture of Maradin's image. The pincushion distortion is visible in the left and right edges, where the horizontal top and bottom edges are perfectly parallel. Therefore, the distorted area is primarily at the left boundary of the image.

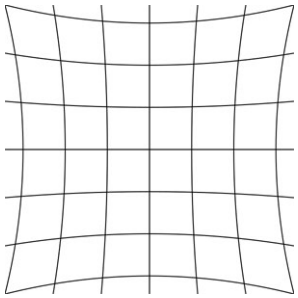

Figure 4: Pincushion Distortion,

Source: http://photographystepbystep.com/wp-content/uploads/2011/09/Pincushion-distortion.jpg

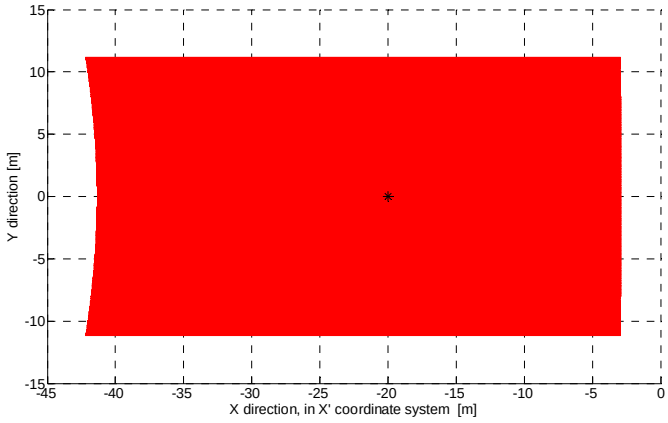

Figure 5: Maradin's Projected Image, obtained by a numerical simulation of the mirror movement

3.2. Parameters definition

We detail the projection parameters that determine the Field of View (FOV):

Table 2: Scan Parameters

Parameters	Definitions
α_L	Laser impinging angle
α_S	Screen impinging angle
$\theta_{peak}^{O_p,x}[rad]$	Maximum ***Horizontal*** Optical Angle - Peak
$\theta_{peak}^{O_p,y}[rad]$	Maximum ***Vertical*** Mechanical Angle - Peak

Additional geometrical properties that are used in Figure 6 include:

- Point O – mirror's center
- Point P – Perpendicular distance in the z direction between the mirror and the screen
- Point A –The projected laser beam spot from the mirror, when the mirror is at rest.
- Point B – The projected laser beam spot, when the mirror is at its maximal rotation angle to the right.
- Point C – The projected laser beam spot, when the mirror is at its maximal rotation angle to the left.

The horizontal distance between the points B-C defines the horizontal field of view.

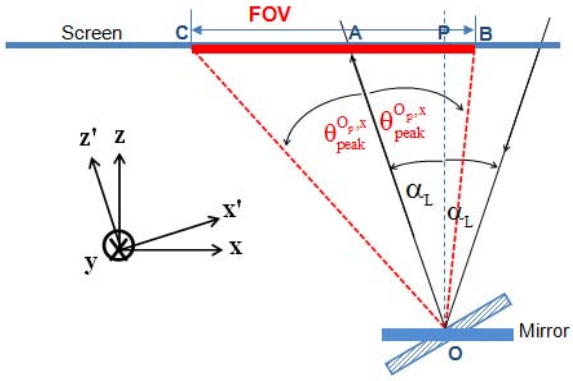

Figure 6: Schematic Sketch of X Axis Field of View (FOV) Parameters

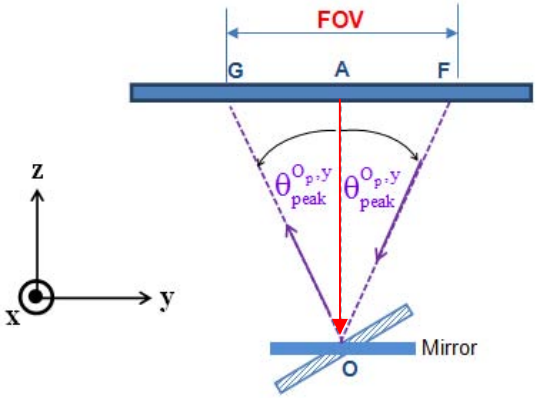

Figure 7: Schematic Sketch of Y Axis Field of View Parameters

Figure 7 depicts the vertical field of view. The laser beam is parallel to the vertical axis (indicated by a red arrow that is pointing towards the mirror's center point) and therefore the vertical FOV is symmetric with respect to the z axis.

Figure 8 depicts a simulation's result of the projected 3D surface (red) and the intersection of the light with a 2D plane (black). The model used for this simulation is based on two rotation matrices, each one representing one rotation angle of the mirror. Consequently, the 3D image is a geometrical result of the dynamic motion of the dual-axis mirror. The four straight lines (dark blue) represent the four vertices of the 3D image, which emphasis the asymmetry of the image, caused due to the impinging-angle of the laser, which deflects the obtained image from the symmetry axis of the mirror.

The intersection between the light rays that create the 3D surface and the screen is calculated using a parameter β, which is a constant describing the extension or compression of the initial vector along the unit vector $\bar{R}_{unit}$:

$$\bar{R}_{unit} = \left[\frac{Rx(i,j)}{R_{mod}}, \frac{Ry(i,j)}{R_{mod}}, \frac{Rz(i,j)}{R_{mod}}\right] \qquad (9)$$

More practically, we search the parameter β for which the new vector $\beta\bar{R}_{unit}$ is located on the screen. We use the x and y

coordinates of the new vector (i.e. $\beta\frac{Rx(i,j)}{R_{mod}},\beta\frac{Ry(i,j)}{R_{mod}}$), and check if $\beta Rz(i,j)/R_{mod}$ is equal to the z coordinate of the screen.

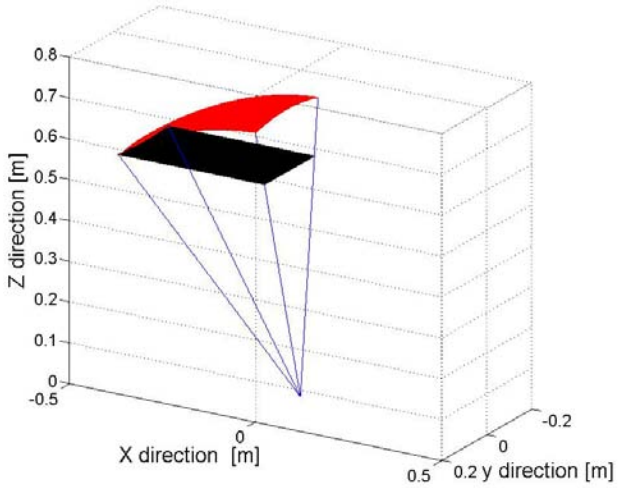

Figure 8: The projected 3D surface from the mirror (red) and the intersection of the image on a 2D plane (black) .

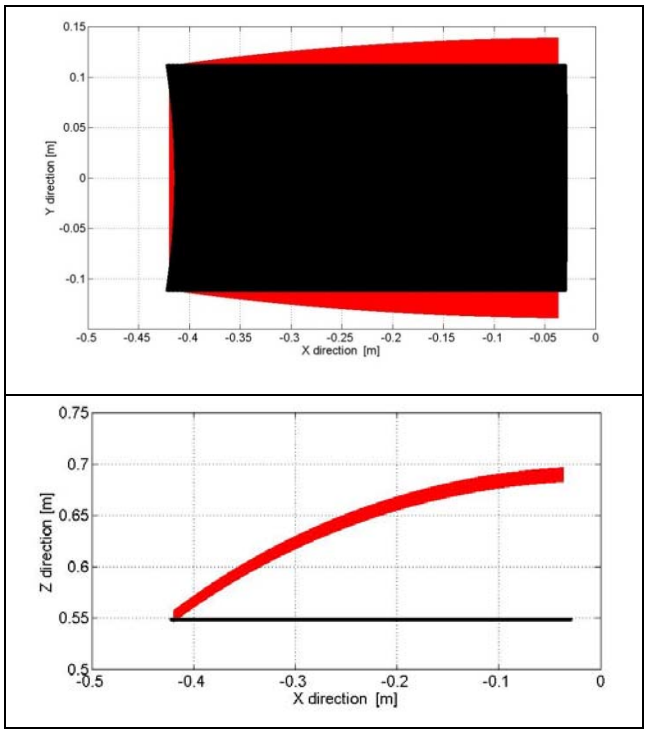

Figure 9: Projection of the X-Y (top) and X-Z (bottom) planes of the 3D surface (red) and the screen (black).

The pincushion distortion, which is visible at the left edge of the projected image (Figure 9, left) is created due to the intersection of a 3D surface onto a 2D plane. The asymmetry of the distortions in both sides of the projected image, which is expressed by a significant pincushion effect on the left boundary and insignificant distortion on the right boundary, is due to the asymmetric laser impinging angle (α_L, see Table 2), which is measured from the symmetry axis of the mirror along the z-axis (see Figure 6) , and causes an offset of the projected surface around this value. Therefore, when calculating the intersection of the light-rays on a 2D plane, the impinging laser angle, as well as the screen angle, defines the geometrics of the obtained image.

4. Conclusion

This paper summarizes two image-correction issues that may be easily implemented into any system that utilizes MEMS-based micro-mirrors as its laser projection element. The laser synchronization that compensates the variable mirror velocity was introduced, as well as the source of the pincushion effect that is derived from kinematics of the mirror.

References

[1] Conant, R. A., Hagelin, P.M., Krishnamoorthy, U. Solgaard, O., Lau K.Y and Muller, R. S., "A raster-scanning full-motion video display using polysilicone micromachined mirror, Transducers '99, The 10th International Conference on Solid-State Sensors and Actuators.

[2] Fisher, M., Giousouf, M., Schaepperle, J., Eichner,D., Weinmann, M., Munch W. von. and Assmus, F., Electrically deflectable polisilicone micromirrors-dynamic behavior and comparison with the results from FEM modeling with ANSYS, *Sensors and Actuators A: Physical*, **67**, 89-95, 1998.

[3] Kawakita, M., Sasaki, H., Arai, J., Okui, M., Okano, F., Haino, Y., Yoshimura, M., and Sato, M., "Projection-type integral 3D display with distortion compensation", *JSID*, **18(**9), 668, 2010.

[4] Milanović, V., Castelino,K., and McCormick, D. Highly Adaptable MEMS-based Display with Wide Projection Angle, 2007 IEEE Int. Conf. on Microelectromechanical Systems (MEMS'07), Kobe, Japan, 2007.

[5] Roscher, K.-U., Grätz, H., Schenk, H., Wolter, A., Lakner, H., "Low cost projection device with a 2-dimensional resonant micro scanning mirror", *Proc. Of SPIE* 5348, 22-31 ,2004.

[6] Schrieber, P., Hoefer, B., Braeuer, A. and Scholles, M., Laser display with single-mirror MEMS scanner, *JSID*, **17**(7), p. 591, 2009.

[7] Specht, H., Kurth, S., Billep, D. and Gessner, T., Analysis of image quality for laser display scanner test, *Proc. Of SPIE* **7206**, 72060G , 2009.

[8] Urey, H., Wine, D. W., and Osborn, T.D., Optical performance requirements for MEMS-scanner based microdisplays, *Proc. Of SPIE* **4178**, 176-185, 2000.